Journal Pre-proof

Freestanding α-Zirconium Phosphate Based Nacre-Like Composite Films Cast from Water

Andrew Smith, Chaoying Wan, Łukasz Figiel, Stefano Farris, Tony McNally

PII: S0266-3538(20)32233-8

DOI: https://doi.org/10.1016/j.compscitech.2020.108443

Reference: CSTE 108443

To appear in: *Composites Science and Technology*

Received Date: 28 May 2020

Revised Date: 21 July 2020

Accepted Date: 25 August 2020

Please cite this article as: Smith A, Wan C, Figiel Ł, Farris S, McNally T, Freestanding α-Zirconium Phosphate Based Nacre-Like Composite Films Cast from Water, *Composites Science and Technology*, https://doi.org/10.1016/j.compscitech.2020.108443.

Tony McNally: Conceptualization, Funding acquisition, Project administration, Methodology, Supervision, Writing- Reviewing and Editing. **Andrew Smith**: Methodology, Investigation, Formal analysis, Data curation, Writing- Original draft preparation. **Chaoying Wan:** Methodology, Supervision, Formal analysis, Writing- Reviewing and Editing. **Lukasz Figiel**: Methodology, Supervision, Formal analysis, Writing- Reviewing and Editing**. Stefano Farris:** Methodology, Investigation, Formal analysis, Writing- Reviewing and Editing.

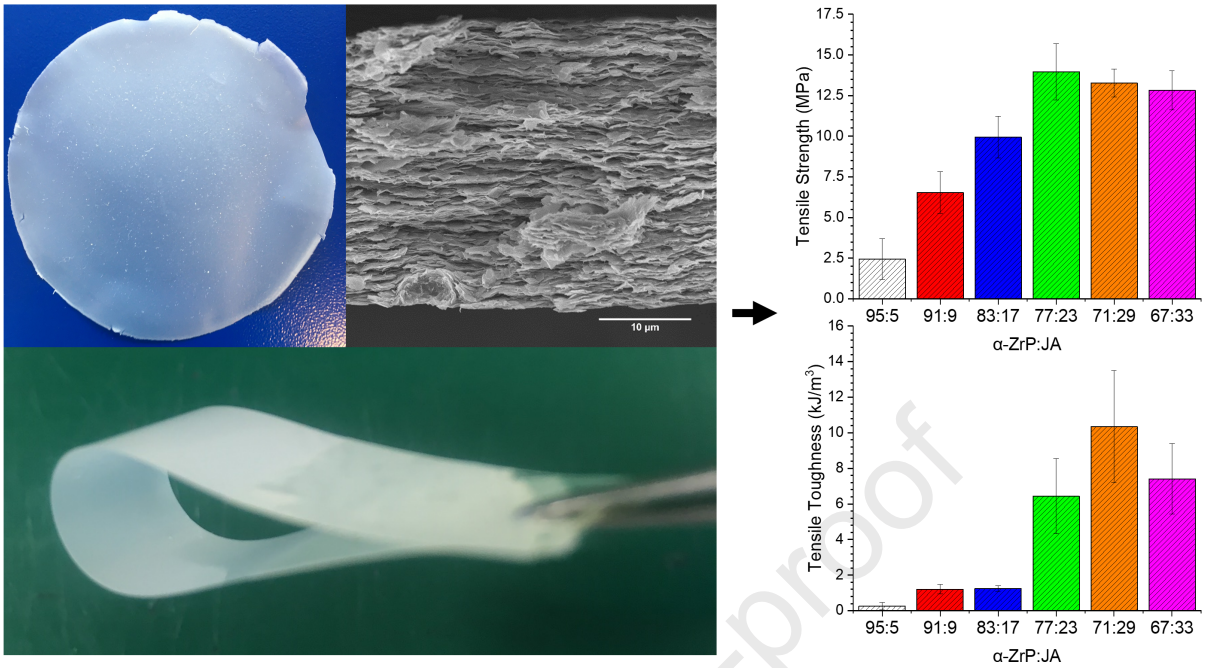

Freestanding α-Zirconium Phosphate Based Nacre-Like Composite Films Cast from Water

Andrew Smith[1], Chaoying Wan[1], Łukasz Figiel[1], Stefano Farris[2], Tony McNally*[1]

[1]International Institute for Nanocomposites Manufacturing (IINM), WMG, University of Warwick, Coventry, CV4 7AL, UK

[2]Department of Food, Environmental and Nutritional Sciences, University of Milan, 20133 Milano, Italy

Abstract

Freestanding nacre-like composite films based on alpha-Zirconium phosphate (α-ZrP) and poly(etheramine) were prepared by casting from water. The α-ZrP nanoplatelets self-assemble and organise to produce a unidirectional nanoplatelet layered structure with the poly(etheramine) acting as both an exfoliating agent and binder for neighbouring nanoplatelets. The terminal amine binds to the α-ZrP through a cationic exchange reaction and once ionically bound, the hydrophobic polyether chain repels the adjacent α-ZrP sheet aiding effective exfoliation. Consequently, the spacing between nanoplatelets increases with increasing poly(etheramine) content. The resultant nacre-like structures can dissipate energy via different mechanisms such that when under tensile or compressive loading significant increases in mechanical properties are possible. Several mechanical property improvements (with respect to the 95:5 composition) were achieved, including a 44- and 200-fold increase in reduced Young' modulus (E_r) and Hardness (H) (from nanoindentation measurements) and, 341% in tensile modulus E, (83:17), 572% in tensile strength σ, (77:23), 707% in maximum strain ε (71:29) and 3981% in tensile toughness U_T, (71:29) (from tensile testing). The barrier performance, to water vapour, of these freestanding nacre-like films per unit

thickness was comparable to several polymers, such as EVOH, Nylon 6,6 and poly(lactic acid)(PLA).

*Corresponding Author: t.mcnally@warwick.ac.uk (Tony McNally)

1. Introduction

Nature continues to be a source of inspiration for researchers due to the variety of material morphologies and unique properties that have evolved over time.[1-3] An excellent example of these is nacre and research interest in this material has grown significantly in recent years. Nacre is an inorganic-organic composite material found in the shell of some molluscs constructed from layered calcium carbonate nanoplatelets and proteins. Alone, the calcium carbonate structure is very weak and so the layers are bonded together using a biopolymer, a protein.[4] Naturally, nacre consists of a minimum of 95% by volume of the inorganic phase with the biopolymer (organic phase) and water making up the remaining 5%. It is due to the unidirectional arrangement of the calcium carbonate nanoplatelets bound by proteins that the 'brick-and-mortar' metaphor is used to describe nacre morphology. It is widely acknowledged that the strong cooperative effects between the rigid nanoplatelet phase and the softer biopolymer phase result in remarkable mechanical properties,[5] achieved by providing the material with a range of different mechanisms to dissipate energy that ultimately increases the total energy that can be absorbed.[6, 7] Researchers are able to replicate these materials through intelligent selection of the two components and innovative production methods. Essentially, it is important to select nanoplatelet and polymer phases with complementary interactions to allow penetration of the polymer between the nanoplatelet layers. This has been attempted with a range of nanoplatelet types[8-13] and polymer materials[14-18] but, significantly more combinations are possible. Production of these films can be simple and often results in materials with very interesting properties.

Zirconium phosphate is an inorganic platelet material that can be prepared having different morphologies. Of these, the alpha form (α-ZrP) is most common and produced through a reflux treatment of zirconium and phosphate salts.[19-22] The alpha form is organised in a layered arrangement where the zirconium ion sits out of the *ab* plane in an alternating 'above' and 'below' conformation.[23] The four oxygens on each phosphate are bound to three different Zr ions forming an octahedral structure. The fourth oxygen points towards the interlayer region at ninety degrees from the plane where it then forms a hydrogen bond with a water molecule in the interlayer cavity. Research into α-ZrP is wide with significant interest focused on the intercalation of molecules between the α-ZrP sheets[24, 25] and the chemical functionalisation possible at these sites.[19, 26, 27] There are also reports of composite materials consisting of unidirectional α-ZrP layers within a polymer matrix[28-30] or in mono- or multi-layer films laid onto substrate surfaces.[19, 25, 27, 31-33] Despite the wealth of research into α-ZrP, there are no reports on freestanding nacre-mimetic materials using these nanoplatelet precursors. Waraich *et al*. reported the production of a nacre-mimetic material using α-ZrP and chitosan.[34] In this work, the authors employed a layer-by-layer (LbL) approach allowing high levels of control over the number of bi-layers present in the final material. From nanoindentation measurements a Young's modulus of 2.6 GPa and a hardness of 70 MPa was achieved however, further tensile mechanical testing could not be completed. Similar work by Han *et al.* explored a LbL approach to produce α-ZrP nacre-mimetic films supported on polymer films with studies focusing on barrier properties towards both oxygen and vanadium.[35, 36]

In this work, we report for the first time the production of freestanding nacre-like films based on α-ZrP through a simple water casting approach. Using this method, relatively transparent films can be produced and tested using universal mechanical testing equipment. A commercial and inexpensive poly(etheramine) is used to intercalate into the α-ZrP interlayer

through ionic-exchange, thus promoting exfoliation and assembly of the layers to form a nacre-like structure. The poly(etheramine) resides in between the layers and also acts as a binder to promote the film formation. The α-ZrP platelet:polymer weight ratios were optimised. The morphology of the resulting nacre-mimetic composites is observed through cross-section scanning-electron microscopy (SEM) to confirm the formation of unidirectional layered structures. The interlayer distance is determined from X-ray diffraction (XRD), thermal stability using thermo-gravimetric analysis (TGA) and mechanical properties measured using both tensile testing and nanoindentation. The water vapour transmission rates (WVTR) of the films were evaluated. Such films may have applications in armour,[37] glass-reinforcement[38] and blast protection,[39] amongst many others.

2. Experimental

2.1 Materials

The α-ZrP nanoplatelets were kindly supplied by the Sunshine Chemical Factory Company, Chengdu, P.R. China and used as received. Poly(etheramine) (Jeffamine M600) having a polyether backbone of propylene oxide and ethylene oxide in a ratio of 9:1, with an approximate molecular weight of 600, was purchased from Merck and used as received.

2.2 Methods

Nacre-like films were produced by first adding α-ZrP (≈500 mg) to deionized water (50 cm^3). A 10 wt% solution of Jeffamine M600 (JA) was produced by dissolving JA (1 g) in deionized water (9 g). The required weight of JA solution was then added to the α-ZrP mixture. The resulting mixture was stirred for 2 hours before being cast into a polystyrene petri-dish and allowed to dry overnight in a fan-assisted oven at 40 °C. Once dry, the films were peeled from the substrate prior to analysis.

2.3 Characterisation

Fourier-transform infrared (FTIR) spectra were recorded on a Bruker Spectrometer with a scan range from 500 cm^{-1} to 4000 cm^{-1}. Scanning Electron Microscopy (SEM) micrographs were obtained using a Zeiss Sigma instrument using an InLens detector at 10kV. The samples were sputter coated using an Au/Pd target. Raman spectroscopy was completed on a Renishaw inVia Raman microscope instrument, using a 532 nm laser in the wavenumber range 100 and 1500 cm^{-1} with a 10-second exposure time, 15 accumulations and the laser power set at 10%. XRD measurements were made using a third generation Malvern Panalytical Empyrean instrument equipped with multicore (iCore/dCore) optics and a Pixcel3D detector operating in 1D scanning mode. A Cu tube was used giving Cu $K_{\alpha 1/2}$ radiation (1.5419 Å) and a beam knife was used to reduce air scatter at the low angles. Scans were recorded in the range 5 – 70 °2θ with a step size of 0.0131° and a counting time of ~ 130 s/step. Thermo-gravimetric analysis (TGA) measurements were completed using a Mettler Toledo TGA1-STARe system under a gentle flow of nitrogen (40-60 cm^3/min). Samples (6-10 mg) were loaded into 70 µL alumina pans and heated from room temperature to 800 °C at a constant rate of 10 K/min. Tensile testing was completed using an Instron 5800R machine equipped with a 500N load cell and an extension rate of 1 mm/min. Test specimens were cut into rectangular strips of width 10 mm and length 40 mm using a razor blade. The thicknesses of the films used was the average of ten (10) measurements made by cross-sectional SEM analysis. The tensile mechanical properties were calculated from an average of five (5) specimens and all tests were completed at room temperature. The Young's modulus was calculated from the gradient of the linear region of the stress-strain curves and the tensile toughness calculated from the area under the stress-strain curves. Nanoindentation measurements were performed using a nanoindentation instrument (Micro Materials Ltd, UK) with a standard Berkovich indenter, which simultaneously measures force and displacement. Measurements were made for each sample at 25 points to a maximum load of

5mN. Deformation of less than 15% of the film thickness was achieved for all samples (except 95:5), avoiding the substrate influencing the results. Reduced Young's modulus (E_r) and hardness (H) were derived from the loading-unloading curve according to the Oliver and Pharr method.[40] Water vapour transmission rate (WVTR, expressed as g m^{-2} $24h^{-1}$) was determined according to the standard method of ASTM F1249 at 38° C and 90% RH. All the tests were carried out with a carrier flow (N_2) of 10 mL min^{-1} and at 59.04 mbar vapour partial pressure difference on the two sides of the specimen. To reset any difference in the transmission rate (TR) values possibly arising from different thicknesses, TR values were converted to a permeability coefficient (P′WV coefficients, respectively) according to equation 1:[41]

$$P'G = PG \times t = \frac{GTR}{\Delta p} \times t \qquad (1)$$

where, P′G is the vapour permeability coefficient (cm^3 μm m^{-2} $24h^{-1}$ atm^{-1}), PG, is the permeance (defined as the ratio of the GTR to the difference between the partial pressure of the vapour on the two sides of the film, Δp), and t is the total thickness of the material.

3. Results and Discussion

FTIR spectroscopy was used to confirm the functional groups present on the α-ZrP (Figure 1 a)). The symmetric P-O stretches of the phosphate group are at 955 cm^{-1} and 1016 cm^{-1} with the asymmetric stretches of the same bond at 1068 cm^{-1} and 1159 cm^{-1}. The P-O-H bending vibration is at 1249 cm^{-1}, the remaining peaks assigned to water in different configurations. The bending, symmetric and asymmetric vibration peaks of bound water in the interlayer space are at 1617 cm^{-1}, 3508 cm^{-1} and 3586 cm^{-1}, respectively. The broad peak at 3127 cm^{-1} corresponds to the stretching vibration of water molecules, most likely adsorbed on the α-ZrP sheets *via* hydrogen bonding.[25, 26, 42]

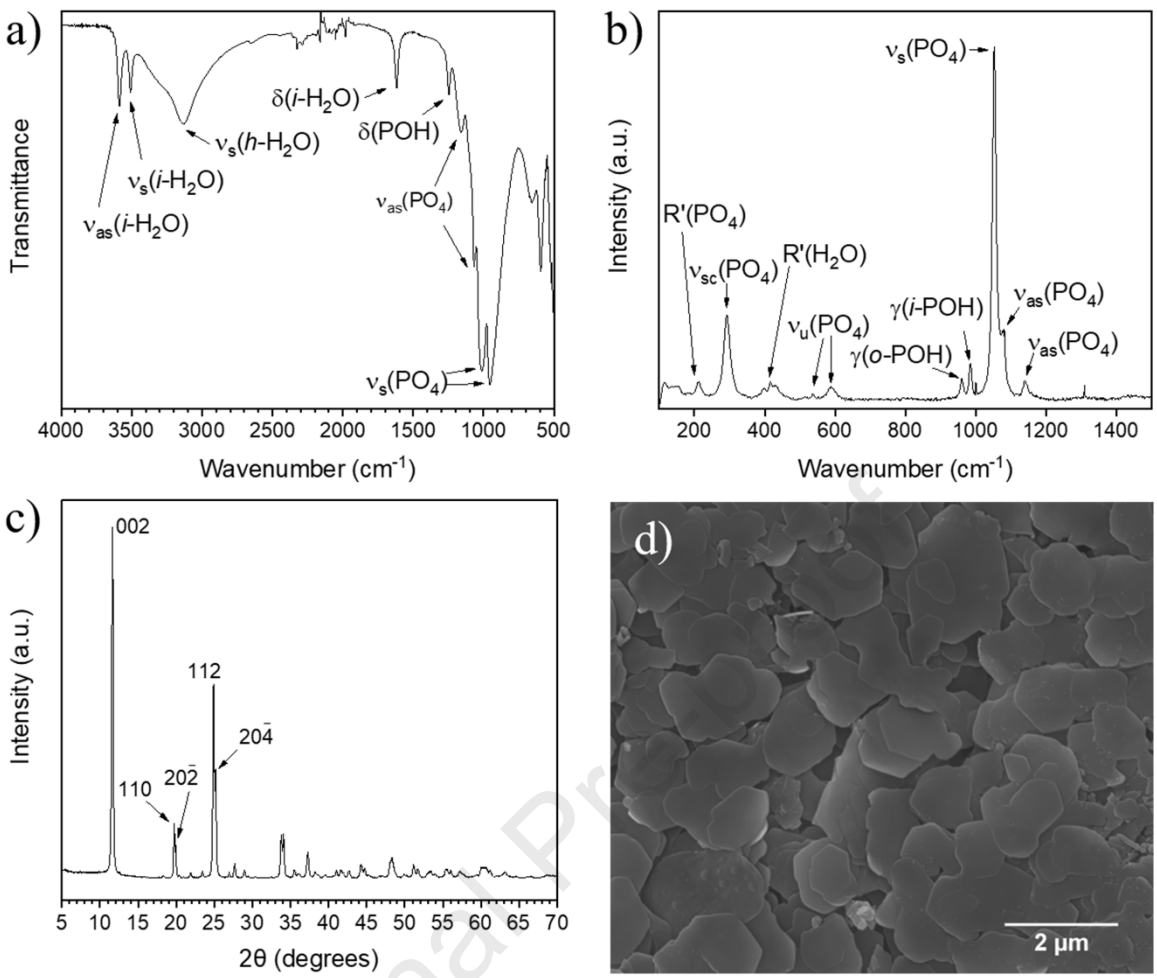

Figure 1. a) FTIR spectrum of the α-ZrP used in this study. (*i*- and *h*- correspond to interlayer and hydrogen-bonded), b) Raman spectrum of α-ZrP. (*i*- and *o*- correspond to in-plane and out-of-plane), c) XRD pattern of α-ZrP with relevant unit cell Miller indices (*hkl*) and d) SEM image of α-ZrP nanoplatelets.

The Raman spectrum for α-ZrP is shown in Figure 1 b) and the relevant peak assignments listed in Table 1. The spectrum displays an intense peak at 1053 cm^{-1} that corresponds to the symmetric stretch of the phosphate group.[43] A 'scissor' stretching vibration is also present at 291 cm^{-1}. Peaks for the asymmetric stretching mode are at 1082 cm^{-1} and 1140 cm^{-1} with a rotational vibration present at 209 cm^{-1}. In-plane and out-of-plane

stretches of the P-O-H groups are at 960 cm^{-1} and 985 cm^{-1}. Finally, a rotational vibration mode of trapped water is at 416 cm^{-1}.[44]

Table 1 – Raman peak assignments.[44]

Wavenumber (cm^{-1})	Functional group	Mode	
209	PO_4	rotation	
291	PO_4	stretch	'scissor'
416	H_2O	rotation	
536	PO_4	stretch	'umbrella'
588	PO_4	stretch	'umbrella'
960	POH	stretch	in-plane
985	POH	stretch	out-of-place
1053	PO_4	stretch	symmetric
1082	PO_4	stretch	asymmetric
1140	PO_4	stretch	asymmetric

The XRD pattern of the α-ZrP nanoplatelets is shown in Figure 1 c). Using the measured diffraction angle, 2θ, the interlayer spacing (d) of a crystalline material can be calculated using Bragg's Law, $n\lambda = 2d\sin\theta$ (where λ = 1.541 Å). In turn, if the unit cell is known, d can be used to determine the cell dimensions. It has been reported previously that the unit cell dimensions of monoclinic α-ZrP vary depending on crystallinity.[45] This can be observed through variation in interlayer distances and more simply through the ratio of intensities of the *hkl* = 002 and 204 peaks (I_{002}:I_{204}).[44] More crystalline α-ZrP displays a more intense *hkl* = 002 peak due to preferred orientation of particles increasing reflection at this angle. From the XRD spectrum, the peaks expected for α-ZrP are all observed and can be assigned below $2\theta = 30°$.[44, 46] The I_{002}:I_{204} ratio is approximately 3:1 which is comparable to the work by Ahrland *et al.*[46] and shows an increase in that reported by Slade *et al.*[44]

SEM imaging of α-ZrP shows the morphology of the nanoplatelets (sheets) and average lateral dimensions, Figure 1 d). The α-ZrP nanoplatelets have rounded edges and

what appears to be a heavily geometric shape.[26] The lateral dimensions were determined from the average measurements of 250 platelets and found to be 1.27 ± 0.43 µm.

Freestanding nacre-like films based on α-ZrP and poly(etheramine) were produced *via* a simple method by casting from aqueous dispersion. The α-ZrP nanoplatelets were first submerged in deionized water and then Jeffamine M600 (JA) added. JA loadings (by weight) were chosen at 1, 5, 9, 17, 23, 29 and 33 wt% to explore the ratios observed in nacre but also at higher polymer loadings to assist exfoliation and in turn improve the homogeneity of the films produced. The polyetheramine (JA) has a single amine group on one terminus of the chain. The surface of α-ZrP is known to be have excellent ion exchange capabilities.[31] During the exfoliation process, the terminal amine is able to bind to the α-ZrP through a cationic exchange reaction. Once ionically bound, the hydrophobic polyether chain repels the adjacent α-ZrP sheet aiding effective exfoliation. Examples of these films are shown in the photographs in Figure 2 a) through f). The films produced with 1wt% JA proved extremely brittle and so couldn't be tested using the same methods as the other films. It should be noted the films begin to become optically transparent at ≥17 wt% JA, which may be useful in certain applications.

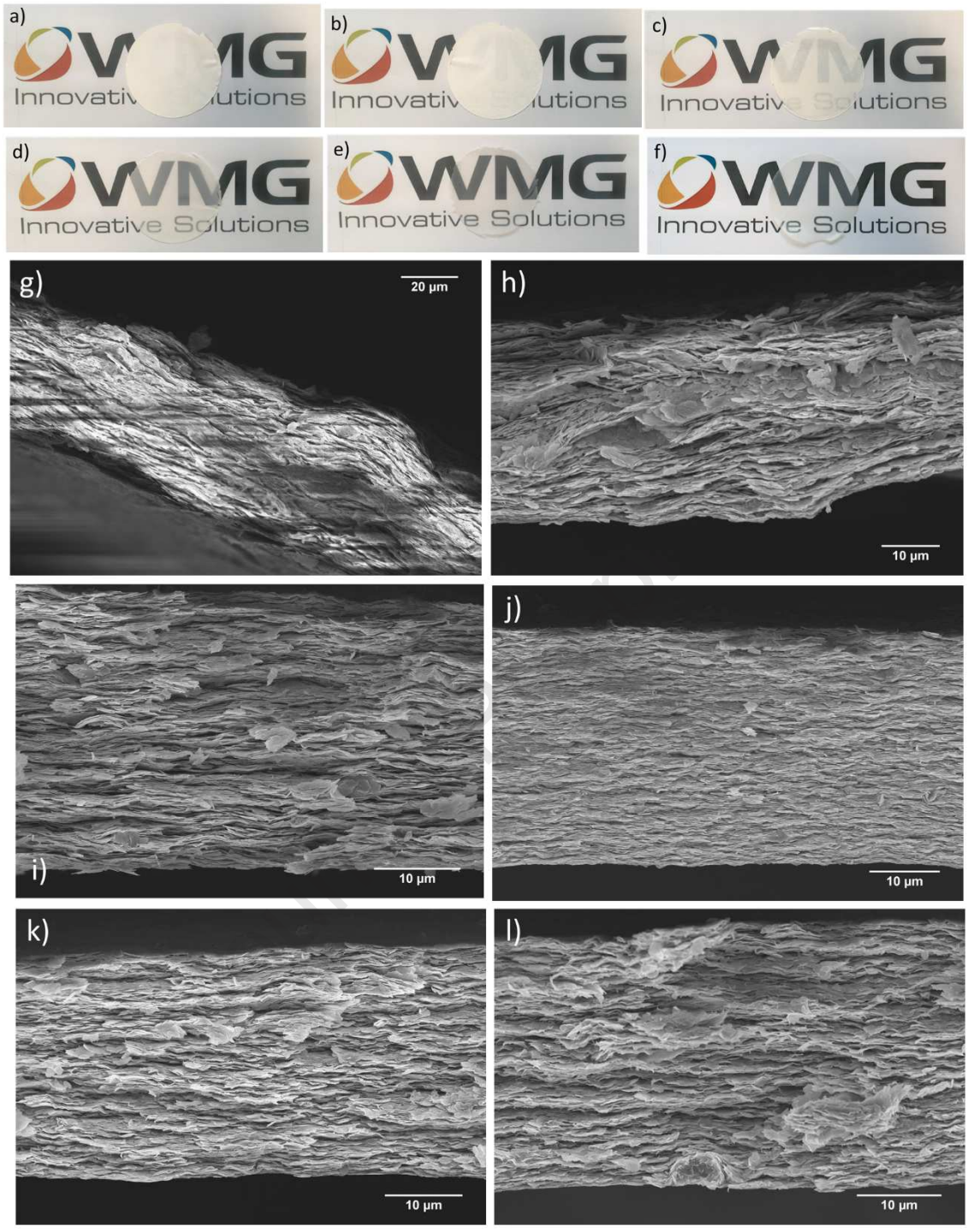

Figure 2. Digital photographs of nacre-like α-ZrP-JA films. (JA loadings are equivalent to a) 5 wt%, b) 9 wt%, c) 17 wt%, d) 23 wt%, e) 29 wt% and f) 33 wt% (all films are approximately 100 mm in diameter) and, cross-section SEM images of α-ZrP films. (JA loadings are equivalent to g) 5 wt%, h) 9 wt%, i) 17 wt% and j) 23 wt%), k) 29 wt% and l) 33 wt%.

Cross-sections of the nacre-like films were imaged using SEM and confirmed a self-assembled unidirectional layered structure. Figure 2 g) through l) shows representative SEM images that show clearly the arrangement of nanoplatelets along a single plane with multiple layers. At lower α-ZrP weight loadings, the layered structure appears less well defined with regions of platelets oriented in different directions. This is likely due to the α-ZrP platelets being less well exfoliated at low JA content. At high 'polymer' content, the volume of JA promotes better exfoliation and so in turn improves homogeneity of the dispersion before casting and yields more organised films, Figure 2 i) – l). For samples with low JA content, the JA does not effectively exfoliate portions of the α-ZrP sheets. As a result, during the self-assembly process, different regions of exfoliated and un-exfoliated α-ZrP result, giving rise to the in-homogeneities observed.

The XRD spectra of the nacre-films provide some interesting insights (Figure 3). As is expected, the *hkl* = 002 peak is observed due to the layered arrangement within the α-ZrP nanoplatelets. Interestingly, a second peak is observed at 2θ = 8-9° that increases in intensity and shifts to lower 2θ with increasing JA content. This corresponds to an increase in the *d*-spacing (Table 2), derived from the larger volumes of JA penetrating between the α-ZrP layers. The increase in the intensity of this peak corresponds to well-exfoliated regions of the nacre-like films and correlates with increasing JA content. This suggests the increase in interlayer spacing is proportional to the volume of JA in the material and not simply because it is present. Poorly exfoliated α-ZrP domains have no distinctive peak, which is symptomatic of a lack of homogeneity that is undetected by XRD. Combined, the XRD data and cross-sectional SEM images confirm that at low JA content (<9 wt%), the films consist of a poorly assembled layered material. In contrast, at higher JA content (>9 wt%) the, α-ZrP is highly exfoliated and self assembles into homogeneous nacre-like films with increased interlayer distances.

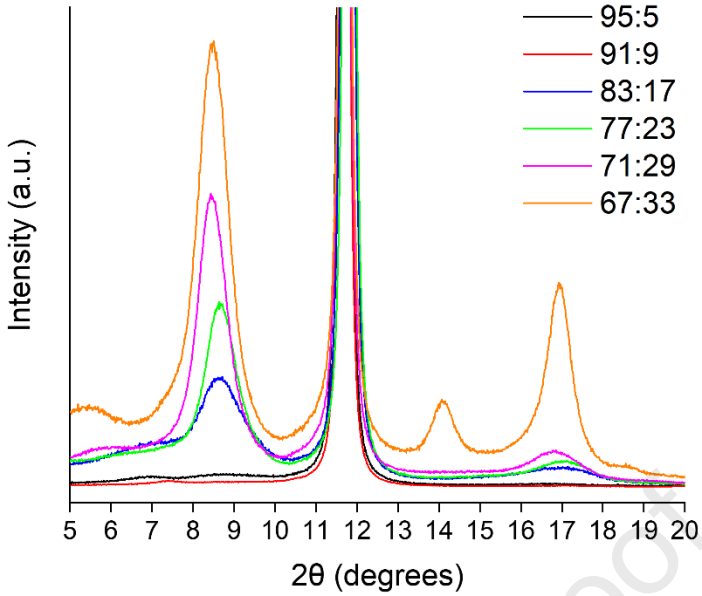

Figure 3. XRD spectra of the α-ZrP-JA nacre-like films. Legend: ratio of α-ZrP:JA.

Table 2. *d* spacings of α-ZrP-JA films determined the peak at 2θ = 8-9° from Figure 3.

Sample	95:5	91:9	83:17	77:23	71:29	67:33
d spacing (nm)	no peak	no peak	1.003	1.008	1.025	1.025

The thermal stability of the films was analysed using TGA, Figure 4. The initial weight loss that can be assigned to the evaporation of interlayer water. The films are all stable until approximately 300 °C at which point the organic JA polymer begins to degrade.[47] The α-ZrP is much more stable and is not fully degraded, even at 800 °C as has been reported previously.[48] Critically, with degradation only beginning at close to 300 °C, these films show good thermal stability and will remain stable in a wide range of engineering environments and applications.

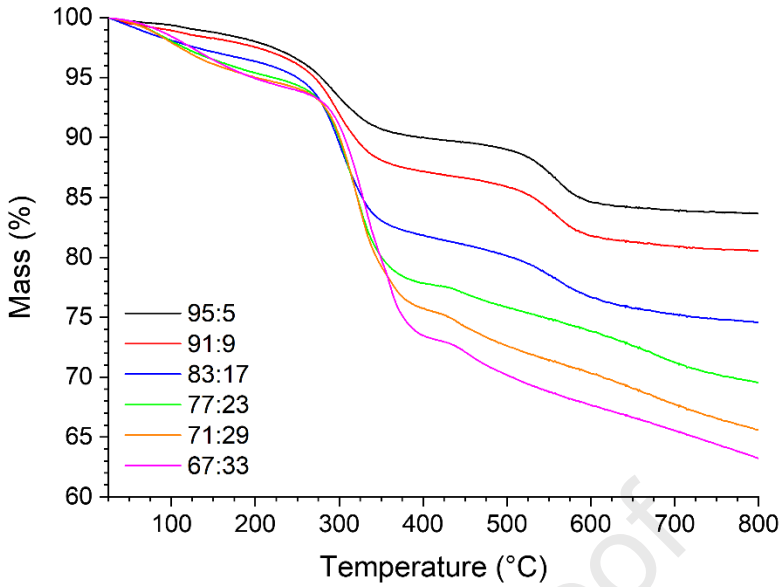

Figure 4. TGA weight loss curves for different αZrP:JA films.

The tensile mechanical properties of the α-ZrP-JA nacre-like films were determined to assess viability for use in engineering applications (Figure 5 and Table 3). Waraich *et al.* were able to complete nanoindentation measurements on polymer supported α-ZrP films but did not report quasi-static tensile properties.[34] Due to the lack of any relevant literature, it is impossible to compare the results of this work to any previous examples. The values obtained for the different mechanical properties are a benchmark for similar materials developed in the future. The Young's modulus of 7.81 ± 2.01 GPa for 83:17 (α-ZrP:JA) was 341% greater than that achieved for the 95:5 film. It has been previously reported that an increase in modulus can be related to the effective stiffening of the polymer phase when incorporated into a material having very high nanofiller content.[49] As the polymer phase penetrates between the nanoplatelet layers, its mobility is constrained by neighbouring nanoplatelets. This has a stiffening effect on the polymer chains reducing thermal motion and increases resistance to tensile deformation. When coupled with favourable interactions between the nanoplatelet and polymer phases, the composite becomes more rigid and results in an increase in Young's modulus. Above 83:17, the modulus reduces with increased JA loading. XRD confirmed an increase in interlayer distance for higher JA loadings and thus confirmed

increased JA content separates the α-ZrP nanoplatelets. It appears that after a critical JA loading, the increased interlayer distance results in a reduction in the stiffening effect as the polymer phase is no longer constrained as strongly by neighbouring α-ZrP nanoplatelets. With increased mobility, the overall stiffness of the material decreases and thus a reduction in modulus results.

Similarly, an increase in tensile strength (σ) is obtained however, the maximum σ value was recorded for the 77:23 material. For this ratio, a tensile strength of 13.96 ± 1.73 MPa was achieved, an increase of 572% over the 95:5 sample. The common failure mechanisms for nacre-mimetic materials are platelet fracture or yielding of the soft interfaces (i.e. the polymer phase).[50] Despite the low loading of polymer in these materials, its behaviour is critical in determining properties. At low JA loadings, yielding of the soft phase occurs through cleavage of polymer and nanoplatelet interactions. Interfacial interactions between the nanoplatelet and polymer phases are more numerous with increasing JA loading due to an increase in binding sites and, an increase in tensile strength results. This is confirmed from the SEM (Figure 2) that displays increasingly amorphous surfaces of the α-ZrP at high JA loading. The amorphous surface morphology is directly related to the increased volume of polymer adhering to the α-ZrP surface due to the increased interactions with JA. Above 77:23, polymer-polymer interactions become more common and the yielding of the soft phase becomes dependant on these interactions. The polymer-polymer interactions (typically van der Waals forces) are weaker than polymer-nanoplatelet interactions (i.e. electrostatic or hydrogen bonding forces) and thus a reduction in tensile strength results.

For both maximum strain and tensile toughness the 71:29 sample had optimal values. Values of 1.06 ± 0.19% and 10.35 ± 3.15 kJ/m^3 represent an increase of 707% and 3981% over that for the 95:5 sample. That the maximum value for each of the different static tensile mechanical properties varied with α-ZrP:JA, 83:17 (modulus), 77:23 (tensile strength) and

71:29 (maximum strain and tensile toughness) is a reflection of the complex energy dissipation mechanisms competing during loading. The modulus is highest at 83:17 due to the relatively low JA content and the stiffness of the nanoplatelets dominates. Further addition of JA results in a reduction in modulus due to the polymer separating more the α-ZrP nanoplatelets resulting in increased chain mobility and interlayer space. At the same time, the number of binding sites between the JA and α-ZrP increases, providing stronger interfacial interactions that improve tensile strength. Further incremental increases of JA introduces more polymer-polymer interactions that facilitate stress failure more readily and consequently, a reduction in tensile strength. Meanwhile, the increased loading of soft phase (JA) provides an increase in maximum strain (and consequently toughness). The material has more capacity to stretch, and so is able to extend further before failure. This effect is observed most prominently for the 71:29 ratio as extension increases to 1.06 ± 0.19%. Ultimately, the reduced interfacial interactions and liquid-like properties of the polymer come to dominate at 67:33, degrading all four properties. α-ZrP nacre-like films display multiple toughening mechanisms.

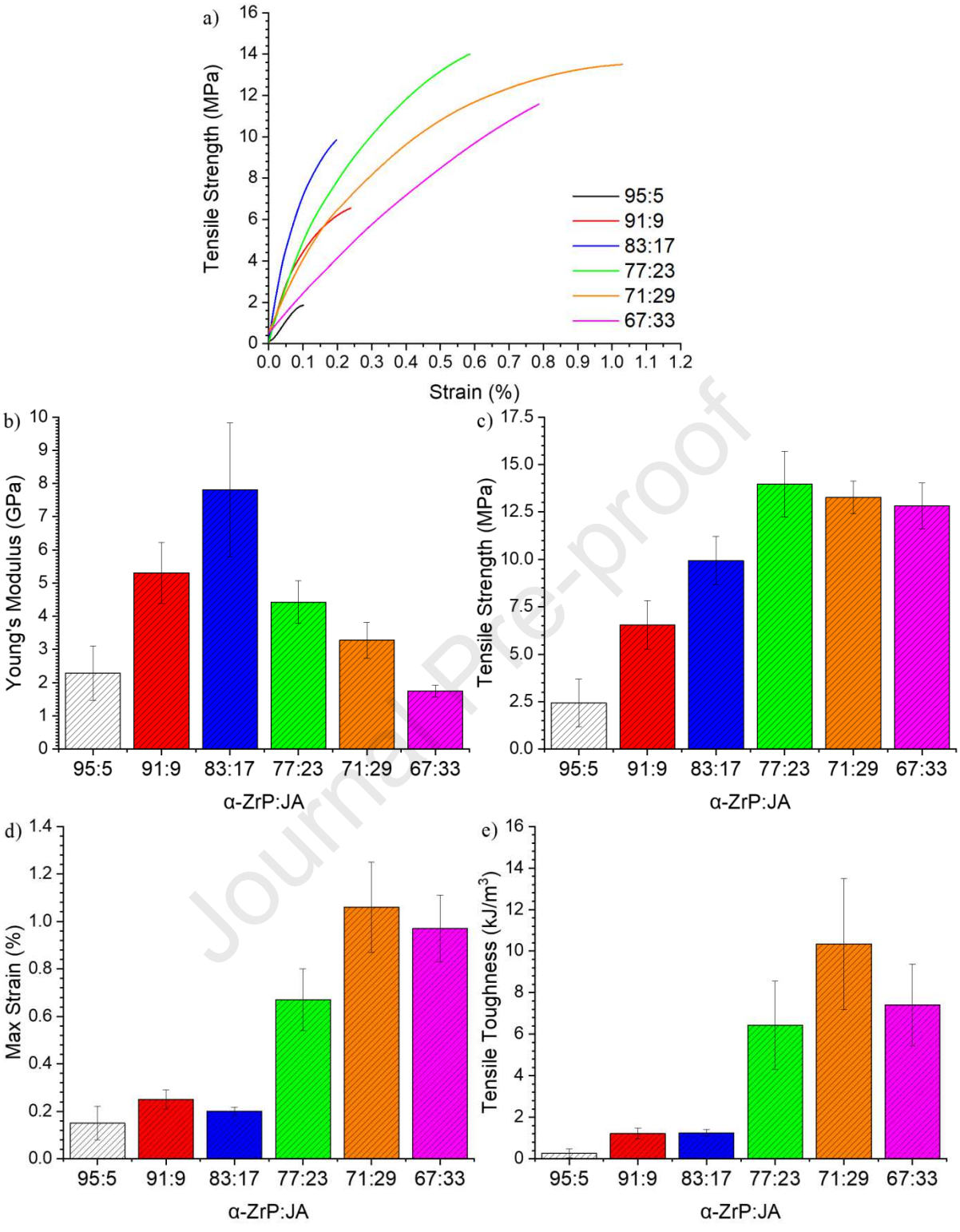

Figure 5. Variation in tensile mechanical properties for α-ZrP:JA nacre-like films where a) representative stress-strain curves for each sample, b) Young's modulus (E), c) tensile strength (σ), d) maximum strain (ε) and e) tensile toughness (U_T).

Table 3. Tensile mechanical properties for α-ZrP-JA samples.

α-ZrP:JA	Young's Modulus, E (GPa)	Tensile Strength, σ (MPa)	Maximum Strain, ε (%)	Tensile Toughness (kJ/m^3)
95:5	2.29 ± 0.82	2.44 ± 1.25	0.15 ± 0.07	0.26 ± 0.21
91:9	5.31 ± 0.92	6.54 ± 1.28	0.25 ± 0.04	1.21 ± 0.26
83:17	7.81 ± 2.01	9.94 ± 1.27	0.20 ± 0.02	1.25 ± 0.16
77:23	4.43 ± 0.64	13.96 ± 1.73	0.67 ± 0.13	6.43 ± 2.12
71:29	3.28 ± 0.54	13.27 ± 0.85	1.06 ± 0.19	10.35 ± 3.15
67:33	1.75 ± 0.18	12.82 ± 1.20	0.97 ± 0.14	7.41 ± 1.97

Nanoindentation experiments were completed and data compared against previous findings, Figure 6. Waraich *et al*. reported a maximum hardness (H) and reduced Young's modulus value (E_r) of 71 MPa and 2.46 GPa, respectively.[34] In this work, the 77:23 α-ZrP:JA nacre-like film has the highest values for both H and E_r (Table 4), H=58.4 ± 9.2 MPa and YM=2.27 ± 0.20 GPa for E_r. Varying the α-ZrP:JA from 95:5 to 77:23 resulted in a 44-fold increase in H and a 200-fold increase in E_r. In this instance, the dual functionality of the polymer phase (JA) acting as both an exfoliating agent and providing strong interfacial interaction with α-ZrP is critical in achieving such mechanical behaviour. Improved exfoliation facilitates a more efficient self-assembly process resulting in more highly ordered alignment of α-ZrP nanoplatelets. Other workers have reported significant increases in mechanical properties of other nacre-mimetic materials utilising chitosan as the polymer phase, [13, 51, 52] attributed to a large number of hydrogen-bonding groups in chitosan forming strong interfacial interactions with the nanoplatelet (nanoclay) phase.[51] The surface of the α-ZrP has a high capacity for hydrogen bonding and so the polymer-nanoplatelet interactions are strong in this material. The JA does not have the same capacity for hydrogen bonding as chitosan and so it is quite remarkable that α-ZrP-JA nacre-like films display comparable properties to those reported with chitosan. It is clear that the α-ZrP sheets provide the bulk of the mechanical strength however, given in this work when the JA loading is low, *H* and E_r are much smaller than when the JA loading is 23 wt%. The cooperative effects of the α-ZrP

nanoplatelet and polymer (JA) is equally as important when the mode of deformation is compressive as in tensile. Due to the positioning of the nanoindenter, the load applied is perpendicular to the α-ZrP nanoplatelets, in contrast to the tensile testing, which is parallel to the platelet direction, Figure 7. As expected, the tensile modulus is larger than that observed from nanoindentation suggesting polymer stiffening observed under tensile load has a greater effect in a parallel (to the applied load) direction. It is possible the compressive deformation during nanoindentation forces the α-ZrP into any pores or imperfections within the film structure reducing the resistance experienced by the tip, yielding a lower modulus value. Increased porosity at low polymer loading has been previously reported by Medina *et al.* for nacre-like films based on clay and cellulose.[53] Under tensile load, the same imperfections should not have a negative impact as the nanoplatelets and polymer are being pulled apart.

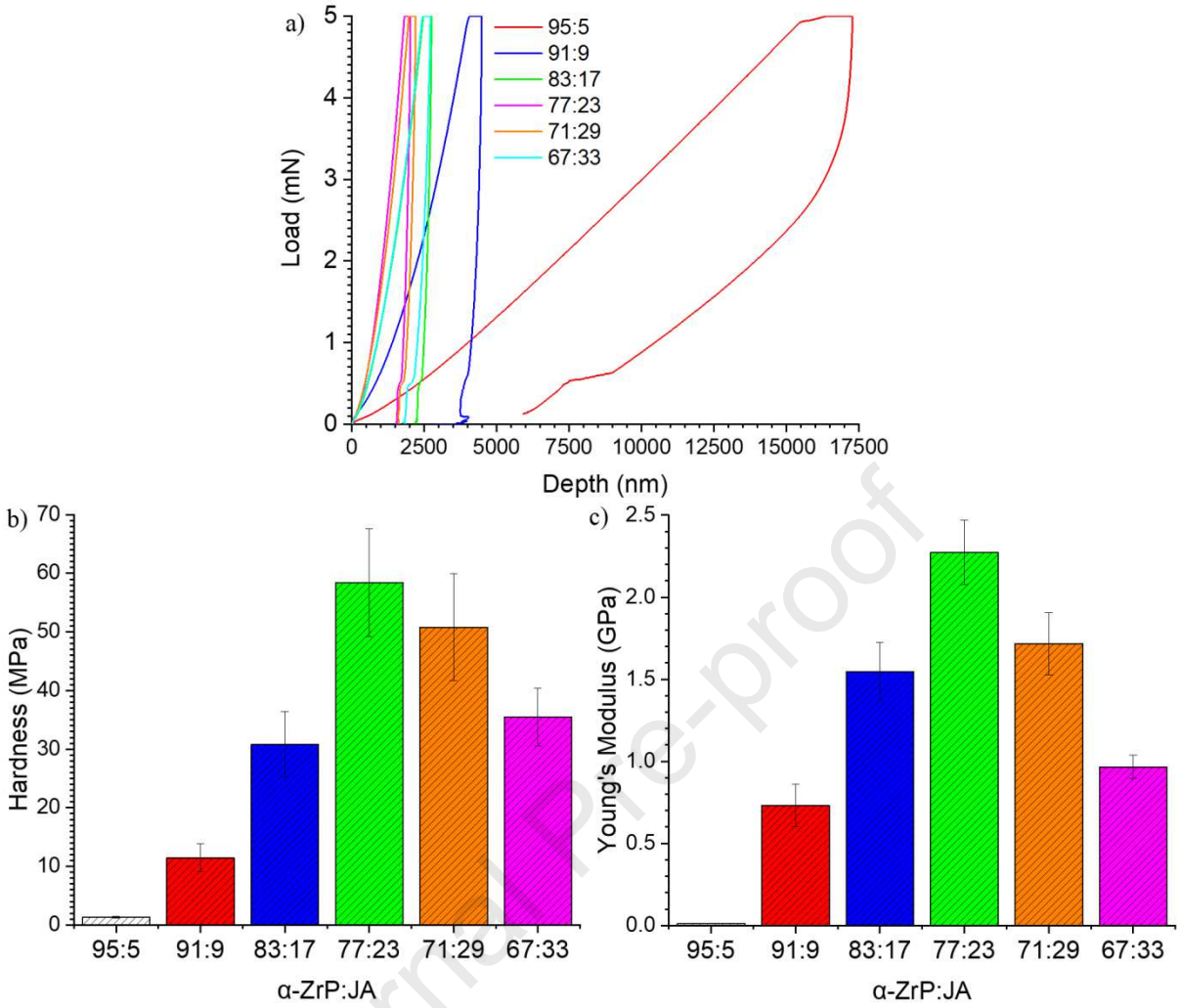

Figure 6. Nanoindentation data for α-ZrP-JA films, a) averaged nanoindentation curves, b) Hardness and c) reduced Young's modulus.

Table 4. Reduced Young's modulus and Hardness values determined from nanoindentation measurements

α-ZrP:JA	Reduced Young's modulus, E_r (GPa)	Hardness, H (MPa)
95:5	$0.01 \pm 6x10^{-4}$	1.32 ± 0.15
91:9	0.73 ± 0.13	11.46 ± 2.40
83:17	1.55 ± 0.18	30.80 ± 5.60
77:23	2.27 ± 0.20	58.40 ± 9.20
71:29	1.71 ± 0.19	50.80 ± 9.10
67:33	0.97 ± 0.07	35.50 ± 4.90

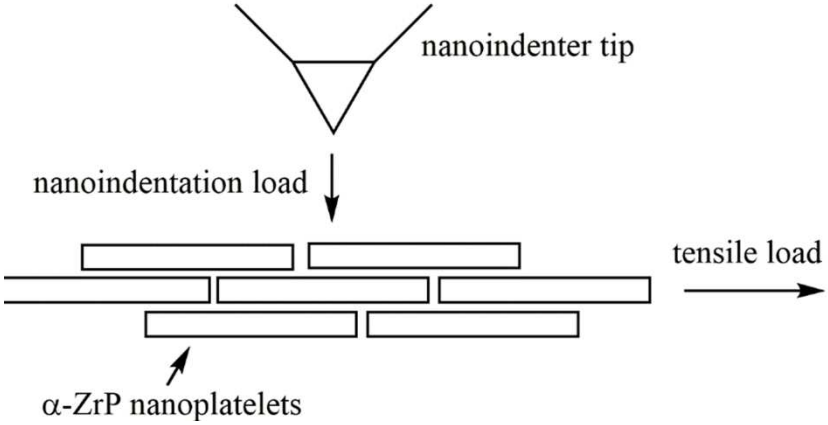

Figure 7. Schematic representation of the direction that the load is applied during nanoindentation (perpendicular) and tensile (parallel) testing.

The water vapour transmission rate (WVTR) of the freestanding nacre-like α-ZrP-JA films was measured and values reported as 'transmission rate' [g/(m^2 24h)], 'permeability' [g μm/(m^2 24h)] and in g mil/(m^2 24h), the latter expressed as 'transmission rate' per unit thickness, see Table 5. The best barrier performance achieved was by the 91:9 sample with a transmission rate per unit thickness of ~243 g mil/(m^2 24h) , approaching that reported for a range of polymer films, including Nylon 6,6,[54, 55] poly(lactic acid),[55] oriented polystyrene[56] and EVOH.[57]

Table 5. WVTR data for different α-ZrP:JA nacre-like films.

Sample α-ZrP:JA	Thickness μm	WVTR g/(m^2 24h)	WVTR g μm/(m^2 24h)	WVTR g mil/(m^2 24h)
95:5	45	1956.687	88050.91	3466.57
91:9	48	128.860	6185.28	243.51
77:23	43	555.393	23881.89	940.23
71:29	37	274.660	10162.42	400.10
67:33	44	358.570	15777.10	621.14

4. Conclusions

Nacre-like films composed of α-ZrP nanoplatelets and a poly(etheramine) (JA) were readily formed via self-assembly by a one-step solution-casting process from an aqueous dispersion. When the JA component was 9 wt% or greater, highly organised reproducible unidirectional nanoplatelet nacre-like films were obtained. The JA acts as both an exfoliating agent for the α-ZrP nanoplatelets and as the 'polymer' phase binding to the nanoplatelets via ionic bonding. The spacing between nanoplatelets increases with increasing JA content. The binding of the α-ZrP nanoplatelets with JA provides a route for the dissipation of energy via different mechanisms when the film is under compressive or tensile loading. This is reflected in the different α-ZrP:JA ratios as to when the optimal mechanical properties were achieved from tensile testing, and in particular, the values for Young's modulus E, tensile strength σ, maximum strain ε and tensile toughness, U_T increased by 341% (83:17), 572% (77:23), 707% (71:29) and 3981% (71:29), respectively, relative to the 95:5 film. From nanoindentation measurements, the highest values for hardness (*H*) and reduced Young's modulus (E_r) were obtained for the 77:23 sample, with H=58.4 ± 9.2 MPa and E_r=2.27 ± 0.20 GPa, a 44-fold and 200-fold increase in H and E_r compared to the 95:5 film. The freestanding 91:9 nacre-like film was the best barrier to water vapour having a transmission rate per unit thickness similar to several polymers, e.g. Nylon 6,6 and EVOH.

Acknowledgements

AS thanks the EPSRC and Jaguar-Land Rover for funding an iCASE Studentship. We acknowledge the Sunshine Chemical Factory Co., Ltd, Chengdu, P.R. China for kindly providing the α-ZrP.

References

(1) Athas, J. C.; Nguyen, C. P.; Zarket, B. C.; Gargava, A.; Nie, Z.; Raghavan, S. R., Enzyme-Triggered Folding of Hydrogels: Toward a Mimic of the Venus Flytrap ACS Applied Materials & Interfaces 2016, 8 (29), 19066-74.

(2) Petrini, M.; Ferrante, M.; Su, B., Fabrication and Characterization of Biomimetic Ceramic/Polymer Composite Materials for Dental Restoration Dental Materials 2013, 29 (4), 375-81.

(3) Zhu, H.; Yang, F.; Li, J.; Guo, Z., High-Efficiency Water Collection on Biomimetic Material with Superwettable Patterns Chemical Communications 2016, 52 (84), 12415-12417.

(4) Marin, F.; Le Roy, N.; Marie, B., The Formation and Mineralization of Mollusk Shell Frontiers in Bioscience 2012, S4 (1), 1099-1125.

(5) Jackson, A. P.; Vincent, J. F.; Turner, R. M., The Mechancial Design of Nacre Proceedings of the Royal Society of London B 1988, 234, 415-440.

(6) Li, L.; Ortiz, C., Pervasive Nanoscale Deformation Twinning as a Catalyst for Efficient Energy Dissipation in a Bioceramic Armour Nature Materials 2014, 13 (5), 501-7.

(7) Smith, B. L.; Schaffer, T. E.; Viani, M.; Thompson, J. B.; Frederick, N. A.; Kindt, J.; Belcher, A.; Stucky, G. D.; Morse, D. E.; Hansma, P. K., Molecular Mechanistic Origin of the Toughness of Natural Adhesives, Fibres and Composites Nature 1999, 399, 761-763.

(8) Li, Y. Q.; Yu, T.; Yang, T. Y.; Zheng, L. X.; Liao, K., Bio-Inspired Nacre-Like Composite Films Based on Graphene with Superior Mechanical, Electrical, and Biocompatible Properties Advanced Materials 2012, 24 (25), 3426-31.

(9) Cui, W.; Li, M.; Liu, J.; Wang, B.; Zhang, C.; Jiang, L.; Cheng, Q., A Strong Integrated Strength and Toughness Artificial Nacre Based on Dopamine Cross-Linked Graphene Oxide ACS Nano 2014, 8 (9), 9511-9517.

(10) Pan, X. F.; Gao, H. L.; Lu, Y.; Wu, C. Y.; Wu, Y. D.; Wang, X. Y.; Pan, Z. Q.; Dong, L.; Song, Y. H.; Cong, H. P.; Yu, S. H., Transforming Ground Mica into High-Performance Biomimetic Polymeric Mica Film Nature Communications 2018, 9 (1), 2974.

(11) Xie, W.; Tadepalli, S.; Park, S. H.; Kazemi-Moridani, A.; Jiang, Q.; Singamaneni, S.; Lee, J. H., Extreme Mechanical Behavior of Nacre-Mimetic Graphene-Oxide and Silk Nanocomposites Nano Letters 2018, 18 (2), 987-993.

(12) Han, J.; Du, G.; Gao, W.; Bai, H., An Anisotropically High Thermal Conductive Boron Nitride/Epoxy Composite Based on Nacre-Mimetic 3D Network Advanced Functional Materials 2019, 29 (13), 1900412.

(13) Liang, B.; Shu, Y.; Wan, P.; Zhao, H.; Dong, S.; Hao, W.; Yin, P., Genipin-Enhanced Nacre-Inspired Montmorillonite-Chitosan Film with Superior Mechanical and UV-Blocking Properties Composites Science and Technology 2019, 182, 107747.

(14) Putz, K. W.; Compton, O. C.; Palmeri, M. J.; Nguyen, S. T.; Brinson, L. C., High-Nanofiller-Content Graphene Oxide-Polymer Nanocomposites via Vacuum-Assisted Self-Assembly Advanced Functional Materials 2010, 20 (19), 3322-3329.

(15) Tian, Y.; Cao, Y.; Wang, Y.; Yang, W.; Feng, J., Realizing Ultrahigh Modulus and High Strength of Macroscopic Graphene Oxide Papers through Crosslinking of Mussel-Inspired Polymers Advanced Materials 2013, 25 (21), 2980-3.

(16) Shahzadi, K.; Mohsin, I.; Wu, L.; Ge, X.; Jiang, Y.; Li, H.; Mu, X., Bio-Based Artificial Nacre with Excellent Mechanical and Barrier Properties Realized by a Facile in Situ Reduction and Cross-Linking Reaction ACS Nano 2017, 11 (1), 325-334.

(17) Wan, S.; Xu, F.; Jiang, L.; Cheng, Q., Superior Fatigue Resistant Bioinspired Graphene-Based Nanocomposite via Synergistic Interfacial Interactions Advanced Functional Materials 2017, 27 (10), 1605636.

(18) Liu, Y.; Shi, X.; Liu, S.; Li, H.; Zhang, H.; Wang, C.; Liang, J.; Chen, Y., Biomimetic Printable Nanocomposite for Healable, Ultrasensitive, Stretchable and Ultradurable Strain Sensor Nano Energy 2019, 63, 103898.

(19) Kaschak, D. M.; Johnson, S. A.; Hooks, D. E.; Kim, H.-N.; Ward, M. D.; Mallouk, T. E., Chemistry on the Edge: A Microscopic Analysis of the Intercalation, Exfoliation, Edge Functionalization and Monolayer Surface Tiling Reactions of α-Zirconium Phosphate Journal of the American Chemical Society 1998, 120, 10887-10894.

(20) Alberti, G.; Casciola, M.; Constantino, U., Inorganic Ion-Exchange Pellicles Obtained by Delamination of α-Zirconium Phosphate Crystals Journal of Colloid and Interface Science 1985, 107 (1), 256-263.

(21) Boo, W.; Sun, L.; Liu, J.; Clearfield, A.; Sue, H.; Mullins, M.; Pham, H., Morphology and Mechanical Behavior of Exfoliated Epoxy/α-Zirconium Phosphate Nanocomposites Composites Science and Technology 2007, 67 (2), 262-269.

(22) Sun, L.; Boo, W. J.; Sue, H.-J.; Clearfield, A., Preparation of α-Zirconium Phosphate Nanoplatelets with Wide Variations in Aspect Ratios New Journal of Chemistry 2007, 31 (1), 39-43.

(23) Troup, J. M.; Clearfield, A., On the Mechanism of Ion Exchange in Zirconium Phosphates. 20. Refinement of the Crystal Structure of α-Zirconium Phosphate Inorganic Chemistry 1977, 16 (12), 3311-3314.

(24) Ha, B.; Char, K.; Jeon, H. S., Intercalation Mechanism and Interlayer Structure of Hexadecylamines in the Confined Space of Layered α-Zirconium Phosphates Journal of Physical Chemistry B 2005, 109, 24434-24440.

(25) Takei, T.; Kobayashi, Y.; Hata, H.; Yonesaki, Y.; Kumada, N.; Kinomura, N.; Mallouk, T. E., Anodic Electrodeposition of Highly Orientated Zirconium Phosphate and Polaniline-Intercalated Zirconium Phosphate Films Journal of the American Chemical Society 2006, 128, 16634-16640.

(26) Huang, H.; Li, M.; Tian, Y.; Xie, Y.; Sheng, X.; Jiang, X.; Zhang, X., Exfoliation and Functionalization of α-Zirconium Phosphate in One Pot for Waterborne Epoxy Coatings with Enhanced Anticorrosion Performance Progress in Organic Coatings 2020, 138, 105390.

(27) Takei, T.; Dong, Q.; Yonesaki, Y.; Kumada, N.; Kinomura, N., Preparation of Hybrid Film of Polyaniline and Organically Pillared Zirconium Phosphate Nanosheet by Electrodeposition Langmuir 2011, 27 (1), 126-31.

(28) Lin, X.; Schmelter, D.; Imanian, S.; Hintze-Bruening, H., Hierarchically Ordered Alpha-Zirconium Phosphate Platelets in Aqueous Phase with Empty Liquid Scientific Reports 2019, 9 (1), 16389.

(29) Wong, M.; Ishige, R.; White, K. L.; Li, P.; Kim, D.; Krishnamoorti, R.; Gunther, R.; Higuchi, T.; Jinnai, H.; Takahara, A.; Nishimura, R.; Sue, H. J., Large-Scale Self-Assembled Zirconium Phosphate Smectic Layers via a Simple Spray-Coating Process Nature Communications 2014, 5, 3589.

(30) Sue, H.-J.; Gam, K. T.; Bestaoui, N.; Spurr, N.; Clearfield, A., Epoxy Nanocomposites Based on the Synthetic α-Zirconium Phosphate Layer Structure Chemistry of Materials 2004, 16, 242-249.

(31) Kerimo, J.; Adams, D. M.; Barbara, P. F.; Kaschak, D. M.; Mallouk, T. E., Nsom Investigtions of the Spectroscopy and Morphology of Self-Assembled Multilayered Thin Films Journal of Physical Chemistry B 1998, 102, 9451-9460.

(32) Kim, H.-N.; Keller, S. W.; Mallouk, T. E.; Schmitt, J.; Decher, G., Characterization of Zirconium Phosphate/Polycation Thin Films Grown by Sequential Adsorption Reaction Chemistry of Materials 1997, 9, 1414-1421.

(33) Carosio, F.; Alongi, J.; Malucelli, G., α-Zirconium Phosphate-Based Nanoarchitectures on Polyester Fabrics through Layer-by-Layer Assembly Journal of Materials Chemistry 2011, 21 (28), 10370.

(34) Waraich, S. M.; Hering, B.; Burghard, Z.; Bill, J.; Behrens, P.; Menzel, H., Fabrication and Characterization of Biocompatible Nacre-Like Structures from Alpha-Zirconium Hydrogen Phosphate Hydrate and Chitosan Journal of Colloid and Interface Science 2012, 367 (1), 74-82.

(35) Han, D.; Luo, Y.; Ju, Q.; Xiao, X.; Xiao, M.; Xiao, N.; Chen, S.; Peng, X.; Wang, S.; Meng, Y., Nano-Brick Wall Architectures Account for Super Oxygen Barrier PET Film by Quadlayer Assembly of Polyelectrolytes and Alpha-Zrp Nanoplatelets Polymers (Basel) 2018, 10 (10), 1082.

(36) Zhang, L.; Ling, L.; Xiao, M.; Han, D.; Wang, S.; Meng, Y., Effectively Suppressing Vanadium Permeation in Vanadium Redox Flow Battery Application with Modified Nafion Membrane with Nacre-Like Nanoarchitectures Journal of Power Sources 2017, 352, 111-117.

(37) Knipprath, C.; Bond, I. P.; Trask, R. S., Biologically Inspired Crack Delocalization in a High Strain-Rate Environment Journal of the Royal Society Interface 2012, 9 (69), 665-76.

(38) Yin, Z.; Hannard, F.; Barthelat, F., Impact-Resistant Nacre-Like Transparent Materials Science 2019, 364, 1260-1263.

(39) Tran, P.; Ngo, T. D.; Mendis, P., Bio-Inspired Composite Structures Subjected to Underwater Impulsive Loading Computational Materials Science 2014, 82, 134-139.

(40) Oliver, W. C.; Pharr, G. M., An Improved Technique for Determining Hardness and Elastic Modulus Using Load and Displacement Sensing Indentation Experiments Journal of Materials Research 1992, 7 (6), 1564-1583.

(41) Cozzolino, C. A.; Cerri, G.; Brundu, A.; Farris, S., Microfibrillated Cellulose (MFC): Pullulan Bionanocomposite Films Cellulose 2014, 21 (6), 4323-4335.

(42) Wei, S.; Lizu, M.; Zhang, X.; Sampathi, J.; Sun, L.; Milner, M. F., Electrospun Poly(Vinyl Alcohol)/α-Zirconium Phosphate Nanocomposite Fibers High Performance Polymers 2012, 25 (1), 25-32.

(43) He, X.; Xiao, H.; Choi, H.; Díaz, A.; Mosby, B.; Clearfield, A.; Liang, H., α-Zirconium Phosphate Nanoplatelets as Lubricant Additives Colloids and Surfaces A: Physicochemical and Engineering Aspects 2014, 452, 32-38.

(44) Slade, R. C. T.; Knowles, J. A.; Jones, D. J.; Roziere, J., The Isomorphous Acid Salts α-$Zr(HPO_4)_2 \cdot H_2O$, α-$Ti(HPO_4)_2 \cdot H_2O$ and α-$Zr(HAsO_4)_2 \cdot H_2O$ - Comparitive Thermochemistry and Vibrational Spectroscopy Solid State Ionics 1997, 96, 9-19.

(45) Clearfield, A.; Kullberg, L.; Oskarsson, A., On the Mechanism of Ion Exchange in Crystalline Zirconium Phosphates. XI. The Variation in Unit Cell Dimensions and Sodium Ion/Hydrogen Ion Exchange Behaviour in Highly Crystalline α-Zirconium Phosphates The Journal of Physical Chemistry 1974, 78 (12), 1150-1153.

(46) Ahrland, S.; Albertsson, J., Inorganic Ion Exchangers VI. The Unit-Cell Dimensions of Crystalline Zirconium Phosphate Acta Chemica Scandinavica 1969, 23 (4), 1446-1447.

(47) Bestaoui, N.; Spurr, N. A.; Clearfield, A., Intercalation of Polyetheramines into α-Zirconium Phosphate Journal of Materials Chemistry 2006, 16 (8), 759-764.

(48) Li, X.; Wang, Z.; Wu, L.; Tsai, T., One-Step in Situ Synthesis of a Novel α-Zirconium Phosphate/Graphene Oxide Hybrid and Its Application in Phenolic Foam with Enhanced Mechanical Strength, Flame Retardancy and Thermal Stability RSC Advances 2016, 6 (78), 74903-74912.

(49) Podsiadlo, P.; Kaushik, A. K.; Arruda, E. M.; Waas, A. M.; Shim, B. S.; Xu, J.; Nadivada, H.; Pumplin, B. G.; Lahann, J.; Ramamoorthy, A.; Kotov, N. A., Ultrastrong and Stiff Layered Polymer Nanocomposites Science 2007, 318, 80-83.

(50) Barthelat, F.; Rabiei, R., Toughness Amplification in Natural Composites Journal of the Mechanics and Physics of Solids 2011, 59 (4), 829-840.

(51) Yao, H. B.; Tan, Z. H.; Fang, H. Y.; Yu, S. H., Artificial Nacre-Like Bionanocomposite Films from the Self-Assembly of Chitosan-Montmorillonite Hybrid Building Blocks Angewandte Chemie International Edition England 2010, 49 (52), 10127-31.

(52) Wan, S.; Peng, J.; Li, Y.; Hu, H.; Jiang, L.; Cheng, Q., Use of Synergistic Interaction to Fabricate Strong, Tough and Conductive Artificial Nacre Based on Graphene Oxide and Chitosan ACS Nano 2015, 9 (10), 9830-9836.

(53) Medina, L.; Nishiyama, Y.; Daicho, K.; Saito, T.; Yan, M.; Berglund, L. A., Nanostructure and Properties of Nacre-Inspired Clay/Cellulose Nanocomposites—Synchrotron X-Ray Scattering Analysis Macromolecules 2019, 52 (8), 3131-3140.

(54) Lim, L.-T.; Britt, I. J.; Tung, M. A., Sorption and Transport of Water Vapor in Nylon 6,6 Film Journal of Applied Polymer Science 1998, 71, 197-206.

(55) Farris, S., Engineering Properties of Packaging Films. In Innovative Packaging of Fruits and Vegetables: Strategies for Safety and Quality Maintenance, Siddiqui, M. W.; Rahman, M. S.; Wani, A. A., Eds. Apple Academic Press, 2018, p 211-226.

(56) Kamper, S. L.; Fennema, O., Water Vapor Permeability of Edible Bilayer Films Journal of Food Science 1984, 49, 1478-1481.

(57) Zhang, Z.; Britt, I. J.; Tung, M. A., Permeation of Oxygen and Water Vapor through EVOH Films as Influenced by Relative Humidity Journal of Applied Polymer Science 2001, 82 (8), 1866-1872.

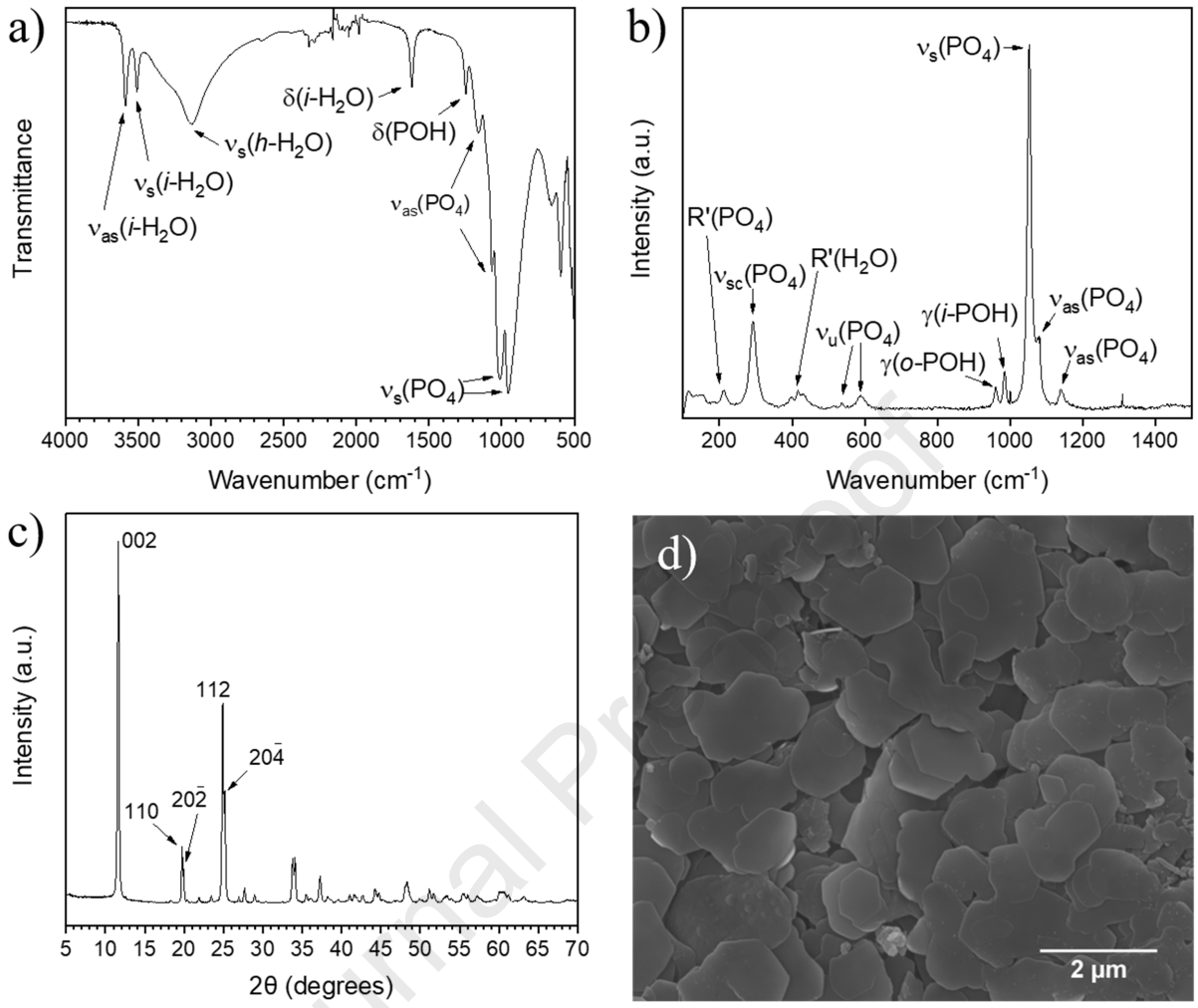

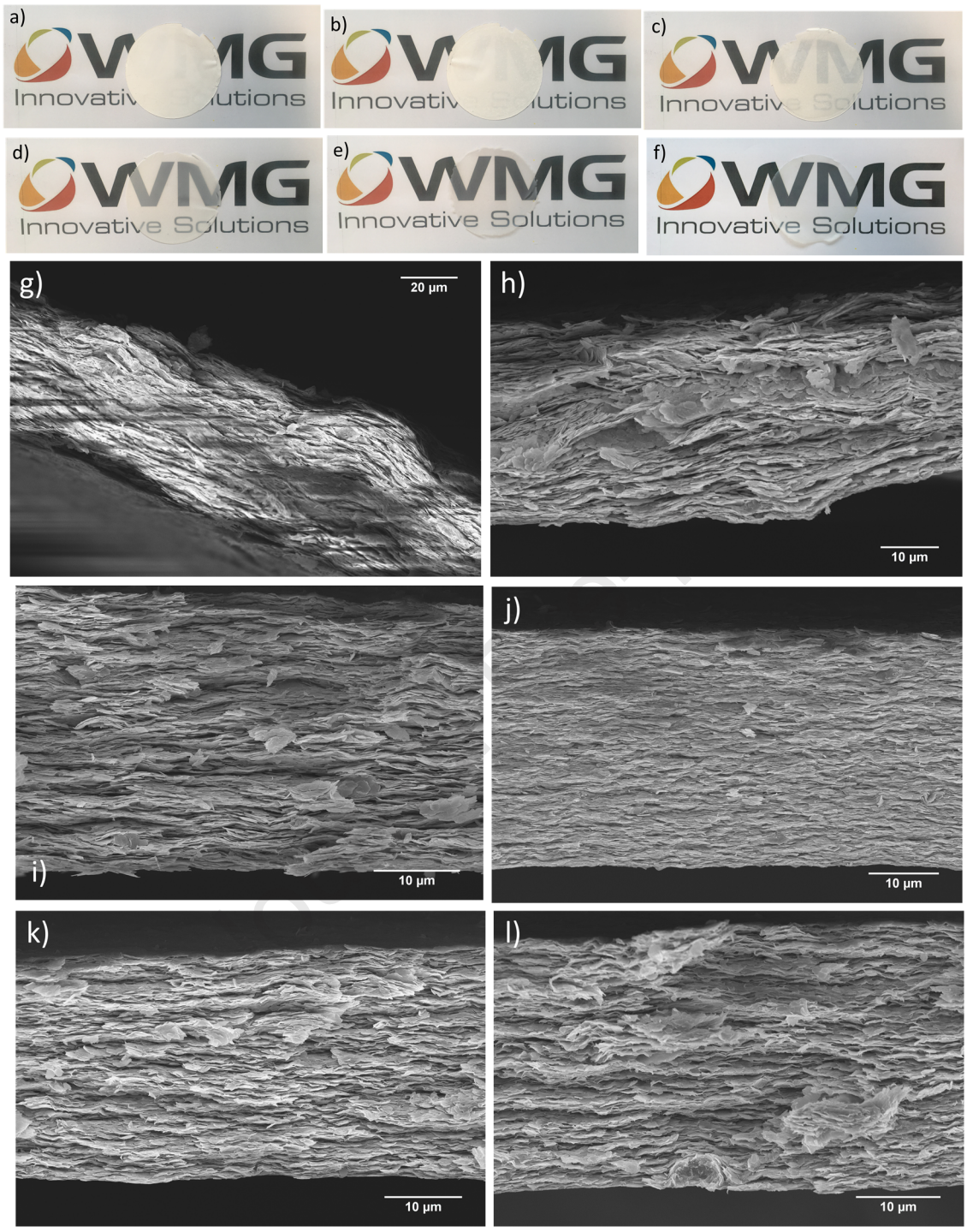
a)
b)
c)
d)
e)
f)
g)
20 µm
h)
10 µm
i)
10 µm
j)
10 µm
k)
10 µm
l)
10 µm

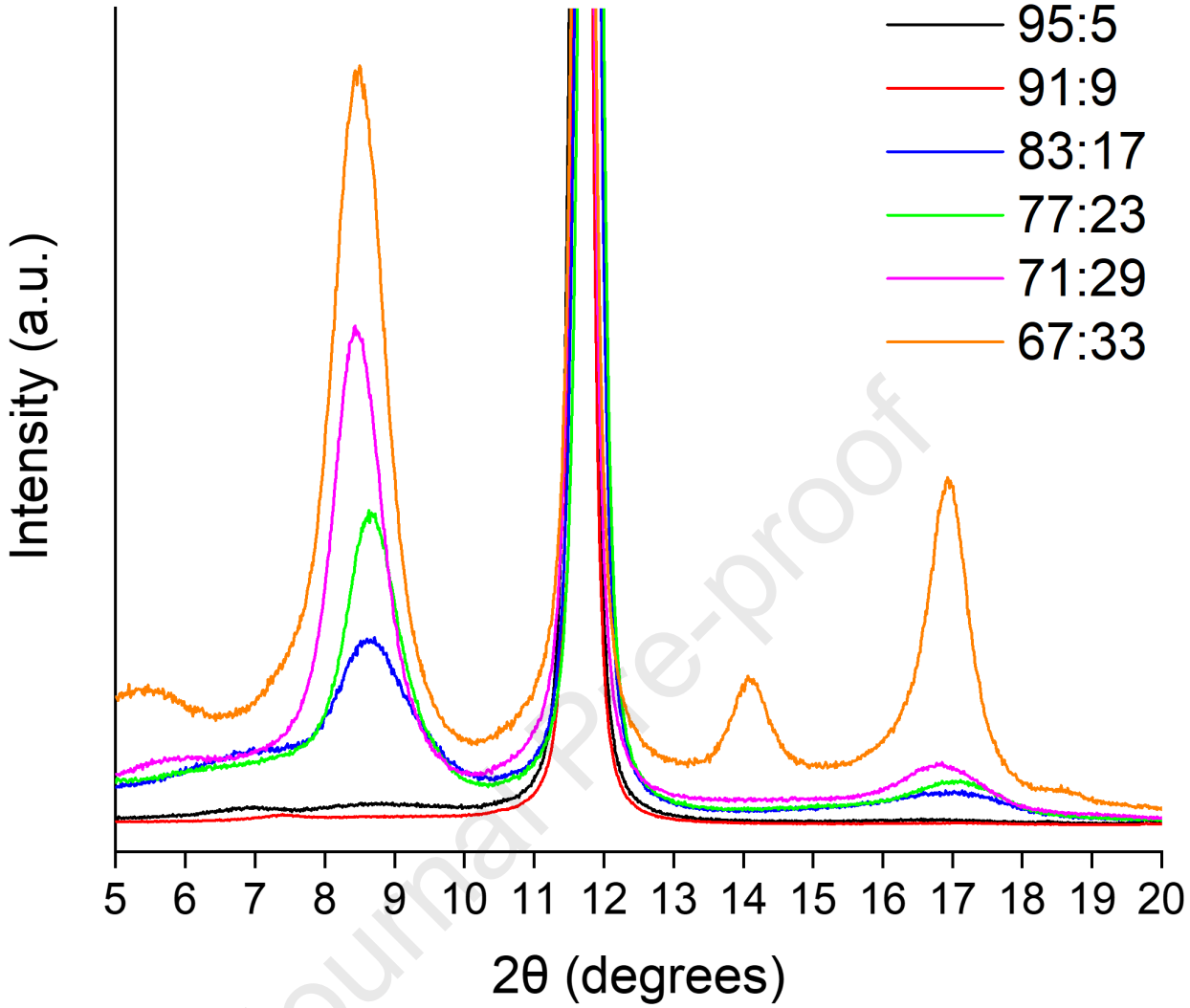

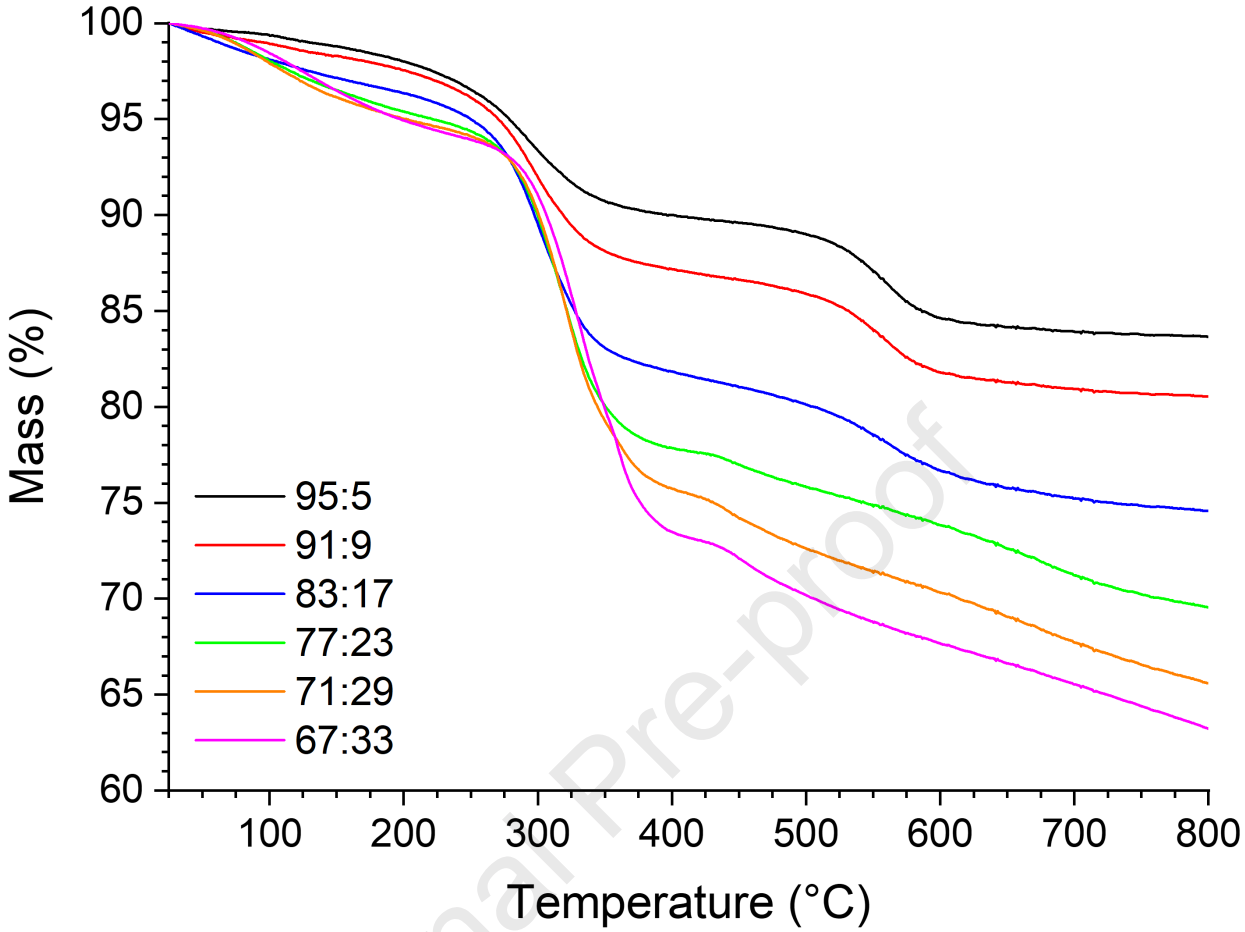

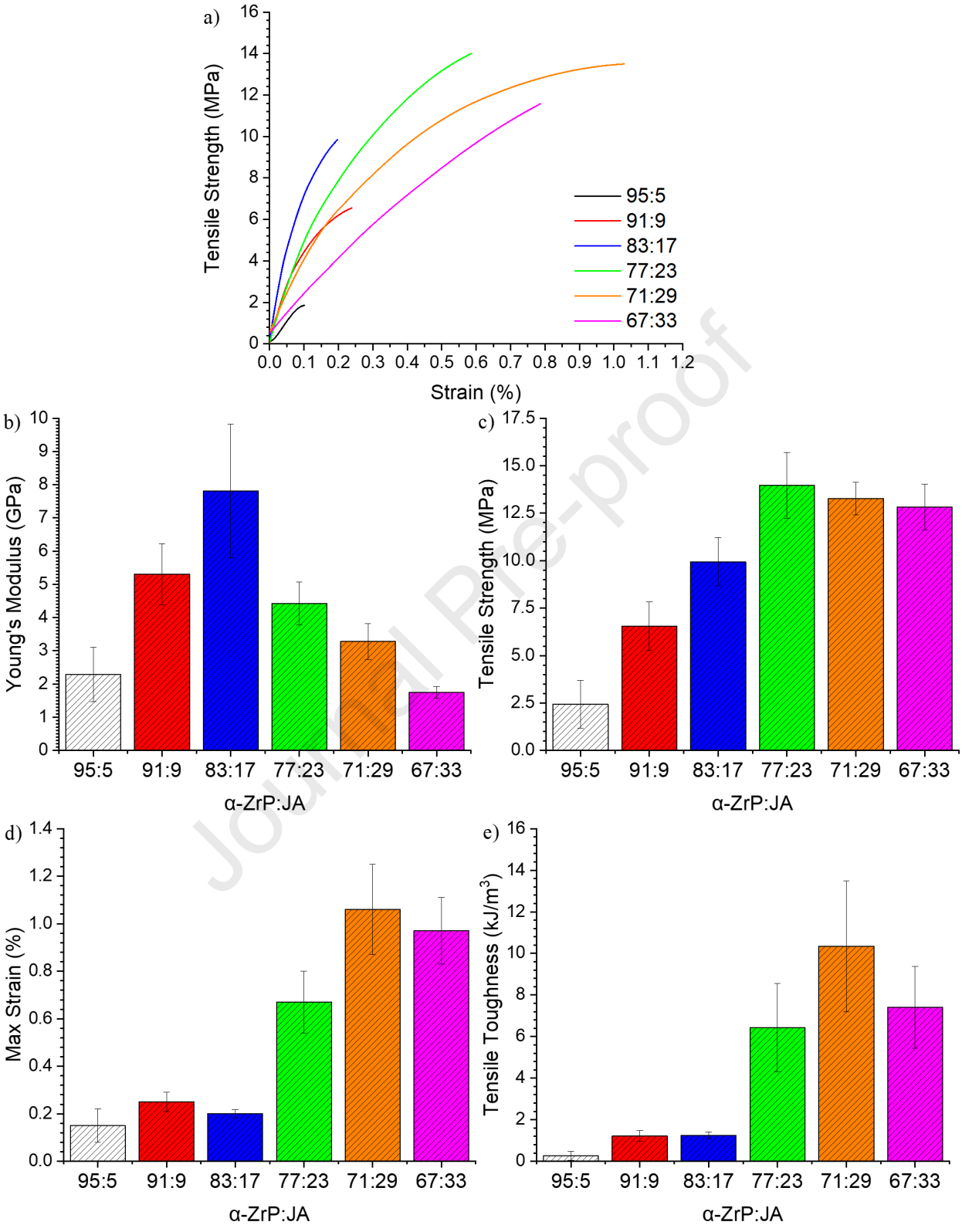

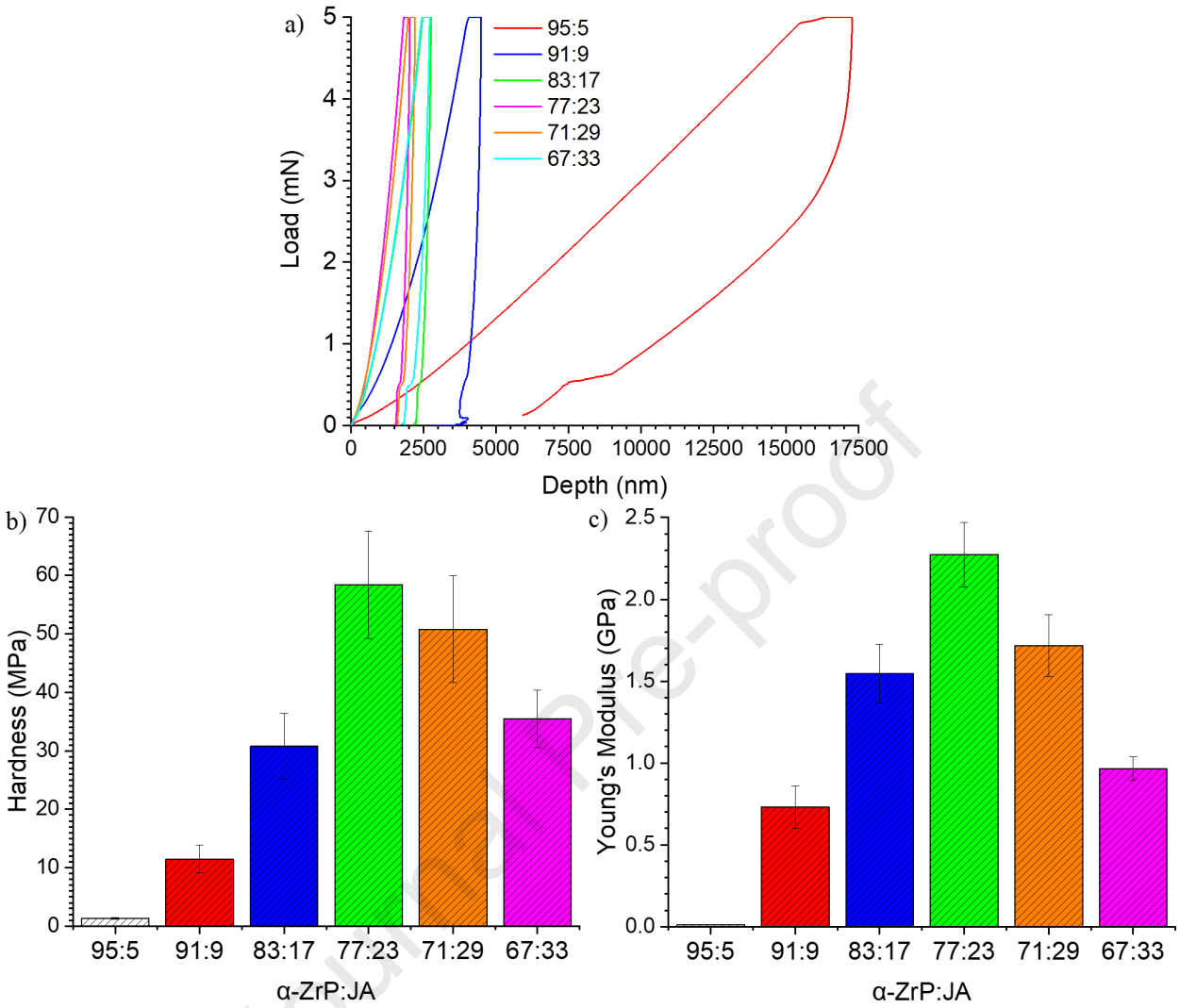

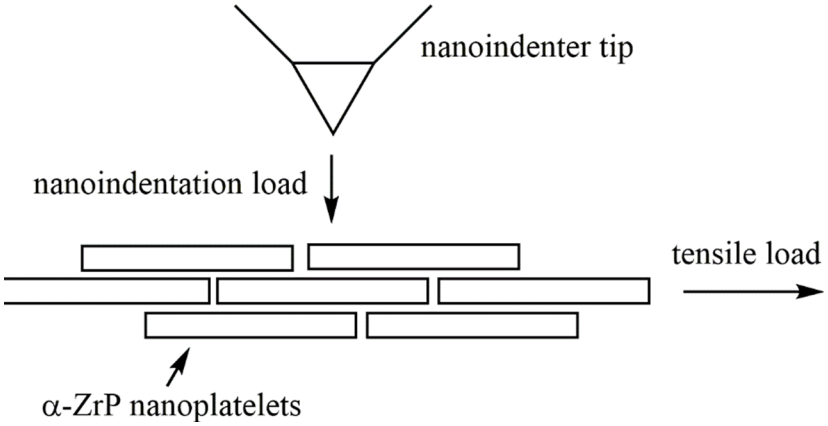

Declaration of interests

☒ The authors declare that they have no known competing financial interests or personal relationships that could have appeared to influence the work reported in this paper.

☐The authors declare the following financial interests/personal relationships which may be considered as potential competing interests: